Mansoura Engineering Journal

Volume 49 | Issue 4 Article 14

2024

Maximum/Minimum Output Current Extraction Based Open-Switch Fault Diagnosis of Voltage Source Inverter

Ahmed S. Gardouh
Department of Electrical Engineering, Faculty of Engineering, Mansoura University, Mansoura, Egypt, ahmed_samir@mans.edu.eg

Eid Gouda
Department of Electrical Engineering, Faculty of Engineering, Mansoura University, Mansoura, Egypt

Abdelhady Ghanem
Department of Electrical Engineering, Faculty of Engineering, Mansoura University, Mansoura, Egypt

ORIGINAL STUDY

Maximum/Minimum Output Current Extraction Based Open-switch Fault Diagnosis of Voltage Source Inverter

Ahmed S. Gardouh*, Eid Gouda, Abdelhady Ghanem

Department of Electrical Engineering, Faculty of Engineering, Mansoura University, Mansoura, Egypt

Abstract

Three-phase induction motor drive systems face significant susceptibility to critical failures arising from open switch faults within the power electronic converter. Implementing monitoring and early fault detection mechanisms for such occurrences not only enhances system reliability but also ensures the safe and uninterrupted operation of the motor drive system. This study introduces an innovative real-time open switch fault detection technique for voltage source inverters fed induction motor drives, leveraging motor stator current analysis. The method aims to track maximum and minimum values of current signals over one cycle. Unlike many current signal-based approaches that require modifications to be integrated with various drive systems, the proposed method operates independently of motor ratings, motor parameters, current levels, and thresholds. Additional characteristics of this approach include simplicity, low computational demands, and fast fault detection capabilities. Both MATLAB simulations and experimental evaluations validate the effectiveness of the proposed fault detection method across various test scenarios.

Keywords: Fault detection, Induction motor, Moving maximum, Moving minimum, Voltage source inverter

1. Introduction

In recent times, induction motor drive systems have successfully tackled the hurdles posed by nonlinear control structure, emerging as the predominant machine type in industrial applications (Eltamaly, 2020; Tran et al., 2021). These systems typically employ Pulse-Width Modulated Voltage Source Inverters (PWM-VSIs) to achieve a broad operational speed range through controlled voltage/frequency ratios (Eltamaly et al., 2010; Chen et al., 2016; Jiang et al., 2017). The complexity of induction motor drive introduces significant challenges in fault diagnosis, primarily due to the dynamic variations in motor operating frequency and load, as well as the intricate control systems in place. As a result, conventional fault diagnosis methods for direct online induction motors are rendered ineffective (Shabbir et al., 2020). Electrical machine drives are susceptible to various faults, including stator, rotor, mechanical, sensor, and power electronic component faults. Based on findings from an industry-based survey (Yang et al., 2011), power semiconductor devices are identified as the most vulnerable components. Failures of power switches can be categorized into two main types: short-circuit faults and open-circuit faults. Short-circuit faults are considered the most severe as they can result in significant damage, prompting drives to incorporate standard protective elements such as fast-acting fuses to mitigate potential catastrophic outcomes (Jlassi and Cardoso, 2019). On the other hand, open-circuit faults may not immediately trigger system shutdown and could persist unnoticed for an extended duration. This situation can lead to excessive strain on the unaffected switches, potentially causing subsequent failures in other components and introducing torque ripples in drives powered by such a faulty inverter.

Received 27 March 2024; revised 1 May 2024; accepted 8 May 2024.
Available online 14 June 2024

* Corresponding author.
E-mail address: ahmed_samir@mans.edu.eg (A.S. Gardouh).

https://doi.org/10.58491/2735-4202.3217

Consequently, the drive system may eventually be forced into shutdown due to subsequent faults, incurring higher repair costs (Wu and Zhao, 2015). Open-circuit faults in inverters typically stem from factors such as heightened electrical or thermal stresses, failures in gate drivers, or disconnections in wiring (Huang et al., 2018). Fault diagnosis techniques for open switches can be classified into three categories: model-based, signal-based, and data-driven approaches.

Data-driven methods diagnose open switch faults by extracting features and classifying faults. In Yang et al. (2023), Open switch fault diagnosis is performed using a combination of fast fourier transform (FFT) and evolutionary neural networks. The adoption of extracting 10 features from each current signal, serving as inputs for a deep neural network used in fault detection within specific motor drives is presented (Yan et al., 2023). While data-driven approaches such as neural networks (Khomfoi and Tolbert, 2007), subtracting clustering (Guan et al., 2007), wavelet-fuzzy networks (Mamat et al., 2006), and data-based methods (Georgakopoulos et al., 2010) have shown improved efficacy, their utility is hindered by significant computational demands, dependency on the availability and quality of data, and prolonged detection periods.

Regarding model-based techniques, they are advantageous for their rapid response and ability to detect in real-time. However, the effectiveness of detection hinges on factors such as model accuracy, threshold settings, and variations in parameters. Open-switch fault detection technique based on Common-mode voltages computed based on the switching average model of VSI fed IM drive system is presented in Cheng et al. (2020). In Wang et al. (2023), the estimation of the quadrature stationary voltage residual component, utilizing the duty cycle signal and healthy model, serves as a robust indicator of faults; however, its applicability is confined to single open switch faults. Employing a differential current observer to derive residuals from the measured and estimated differential currents is presented in Zhou et al. (2020). The diagnostic variables are obtained through feature extraction of these residuals, incorporating an adaptive threshold. This method is limited to detecting single open switch faults.

Other techniques based on signal analysis are divided into current based and voltage-based approaches. Current-based techniques have been presented in Yu et al. (2014); Wu and Zhao (2015); Shadlu (2017); Trabelsi et al. (2017); Zhou et al. (2022); Sun et al. (2023); Suti and Di Rito (2024). A fault diagnosis method is suggested in Wu and Zhao (2015) for detecting open circuits in single and multiple switches through allelic points analysis. However, it imposes a significant computational burden and necessitates remarkable tuning. In Yu et al. (2014), a modified three-phase average current tactic is introduced to pinpoint either single or double open-switch faults across diverse legs. By analyzing the normalized mean values of the motor current in $\alpha\beta$ reference frame during healthy and faulty conditions, open-switch faults can be detected as in Trabelsi et al. (2017). In Shadlu (2017), the detection and diagnosis of open switch faults involve the utilization of Principal Component Analysis in conjunction with the three-dimensional current trajectory. This method overlooks variations in load conditions, leading to false alarms during transient states. In Sun et al. (2023), to normalize current readings, the signals are sampled using a sliding window technique, followed by variable-length normalization to mitigate the impact of fluctuations in current. Following this, the Discrete Fourier transform is applied to extract amplitude and frequency components from the sampled signal. Subsequently, employing Principal Component Analysis, the frequency domain data undergo dimension reduction and feature extraction. This enables the diagnosis of both single and multiple switches, albeit with notable considerable computational demands. In Zhou et al. (2022), decomposing the current signal into its seasonal and trend components involves the utilization of two predefined indices. These indices enable the detection of nine open switch fault cases. Literature (Suti and Di Rito, 2024) employs elliptical fittings to reconstruct current trajectories in the Clarke plane. It utilizes the center of the ellipse and the disparity between their major and minor axes to detect and diagnose only single open switch faults.

To expedite detection, voltage-based methods are employed; however, they necessitate additional voltage sensors, thereby elevating the overall cost. A comparative study of two voltage-based diagnosis methods utilizing extra hardware is presented in Wang et al. (2016). The first approach utilizes pole voltage, while the other employs line voltage. The method proposed by Xu and Yu (2022) utilizes the analysis of the filtered line-to-line voltage of the VSI to detect open circuit faults. In addition, other methods have combined different techniques for more accurate fault detection. In An et al. (2013), Fault detection is accomplished through the analysis of voltage error, which signifies the difference between voltage values estimated by the model and measured voltage values.

This paper presents a novel technique for detecting and diagnosing open switch faults by monitoring the maximum and minimum values of three-phase currents per cycle. The main contributions of this paper are concluded as follows:

(a) Unlike many current signal-based approaches that require modifications to be integrated with various drive systems, the proposed method operates independently of motor ratings, motor parameters, current levels, and thresholds.
(b) The proposed method can detect both single and multiple open switches in addition to open phase faults.
(c) The proposed approach offers several advantages: simplicity, robustness against misdiagnosis stemming from load changes, low computational complexity, and elimination of the necessity for additional sensors.

The organization of this paper is as follows: section II presents the system description and outlines the application of the sliding window technique to identify both maximum and minimum points. Section III introduces the proposed method. Simulation results are outlined in section IV, while section V presents experimental results. Lastly, section VI offers conclusions drawn from the study.

1.1. System description

1.1.1. Structure of voltage source inverter (VSI)

Figure 1 depicts the schematic of a two-level VSI fed a three-phase Induction Motor (IM). The configuration involves the control of the motor speed, and its stator phase currents monitoring. The motor phase currents are utilized based on the proposed approach for open switch faults diagnosis.

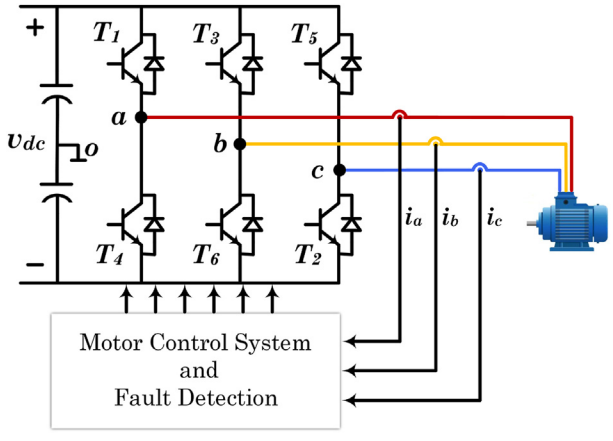

Fig. 1. Voltage source inverter induction motor drive system.

V_{dc} implies the dc input voltage for the drive system, with capacitors for suppressing high-frequency harmonics in the supply voltage. The set of $(T_i, i = 1:6)$ denotes six power transistors, serving as basic elements within the drive system. Similarly, $(D_i,\ i = 1:6)$ indicates six freewheeling diodes aimed at mitigating the effects resulting from inductive rotating loads. PWM signals are produced to alternate the operational states between 'on' and 'off', facilitating the conversion of DC to AC energy. Under normal conditions, the three-phase currents exhibit sinusoidal behavior, sharing identical frequencies and amplitudes, with a phase difference of $2\pi/3$ between any two of them. In cases of faults with an open-loop control strategy, the phase currents of healthy legs remain unaltered, while the phase current of the affected leg becomes distorted. Conversely, in situations where a closed-loop control strategy is employed during a fault, the phase currents of healthy legs will be influenced by the phase current of the affected leg due to the feedback mechanism.

1.1.2. Sliding window method for finding maximum and minimum values

A quick and effective method for determining the maximum or minimum value in a data stream is the sliding window technique. The fundamental concept is to keep a fixed-size window over the data stream. Depending on the issue being solved, the window may be advanced one element at a time or a greater distance. The highest or least value inside the window is calculated at each step. The sliding window method for determining the highest and least value in a data stream is demonstrated as follows:

Consider a currents samples per cycle represented by

$$\left[i_{x(1)}, i_{x(2)}, i_{x(3)}, i_{(4)}, \ldots, i_{x(n)}\right], x = a, b, c$$

$$n = f_{samp} \times T$$

Where f_{samp} is the sample frequency, T is current signal period and n represents the width of the sliding window.

As new data arrives, it enters the window from the right side, while older data exits from the left side as it expires as shown in Fig. 2. The determination of the maximum or minimum value occurs when a new data arrives at the sliding window and when an old one exits. Further elaboration on these calculations is provided below:

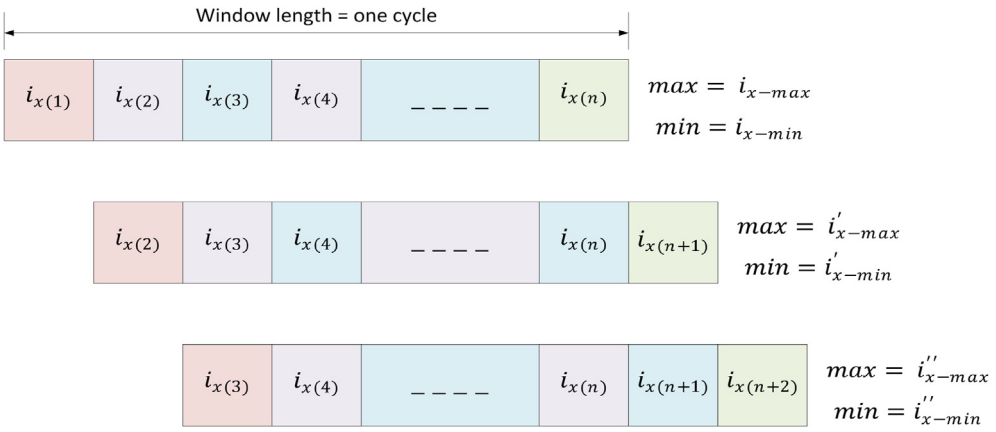

Fig. 2. Finding maximum and minimum current values over one cycle utilizing the sliding window technique.

$$i'_{x-max} = \begin{cases} i_{x-new}, i_{x-new} \geq i_{x-max} \\ i_{x-max}, i_{x-new} < i_{x-max} \end{cases}$$

$$i'_{x-min} = \begin{cases} i_{x-min}, i_{x-new} > i_{x-max} \\ i_{x-new}, i_{x-new} \leq i_{x-max} \end{cases}$$

1.2. Fault diagnosis approach

Three-phase currents are first sampled, following which sliding windows, each spanning one cycle, are employed to ascertain the maximum and minimum values of the current samples for each line current. When a single switch is open, the current associated with that switch forfeits either its positive or negative half-cycle, depending on whether the switch is upper or lower. In the event of the upper switch being open, the corresponding current signal loses its positive half-cycle, resulting in a maximum value of zero for the current cycle. Conversely, if the lower switch is open, the corresponding current signal loses its negative half-cycle, thereby resulting in a minimum value of zero for the current cycle.

1.3. Simulation results

The setup illustrated in Fig. 1 is simulated in MATLAB/Simulink, incorporating the proposed open switch fault detection method. For the investigations, a 3-kW induction motor is supplied by a two-level VSI, with system parameters outlined in Table 1.

Initially, the motor is started without any load, and at t = 1 s, it is loaded with its full-load torque. Subsequently, at t = 2 s, various scenarios of open switch (es) are introduced, and the results are examined as follows:

Table 1. Motor parameters.

Symbol	Parameter	Value	Unit
Induction motor			
P_n	Nominal power	3	KW
V_{LL}	Nominal voltage	400	V
F	Nominal frequency	50	Hz
P	Number of pole pairs	2	
L_{ls}	Stator leakage inductance	10.3	mH
r_s	Stator resistance	2.34	Ω
L_{lr}	Rotor leakage inductance	10.3	mH
r_r	Rotor resistance	1.7	Ω
L_m	Magnetizing inductance	345	mH
B	Friction constant	0.0068	Nm.s
H	Inertia constant	0.0588	Nm.s^2
VSI			
v_{dc}	DC Link voltage	800	V
f_{sw}	Switching frequency	10	KHz

1.4. Single open switch

To validate the autonomy of the proposed method from loading transients and variations in loading ratio, the motor was loaded to its full capacity at t = 1 s, as depicted in Fig. 3.

Observably, both the maximum and minimum values increased in magnitude, consequently moving further away from the zero value that indicates a fault occurrence. When the T_1 switch fault occurs at t = 2 s, the value of i_{a-max} drops to zero as shown in Fig. 3c. Subsequently, the remaining maximum current values increase, and the current minimum values undergo changes, yet they remain significantly distant from zero as shown in Fig. 3c and d. In Fig. 4, the motor is operating under no load conditions, and at t = 2 s, switch T_1 is intentionally opened. As illustrated in Fig. 4c, it is observable that the value of i_{a-max} also decreases to zero, akin to the previous full load condition.

Figure 5 depicts the values of $i_{abc-max}$ and $i_{abc-min}$ when the lower switch T_4 is faulty. In this scenario,

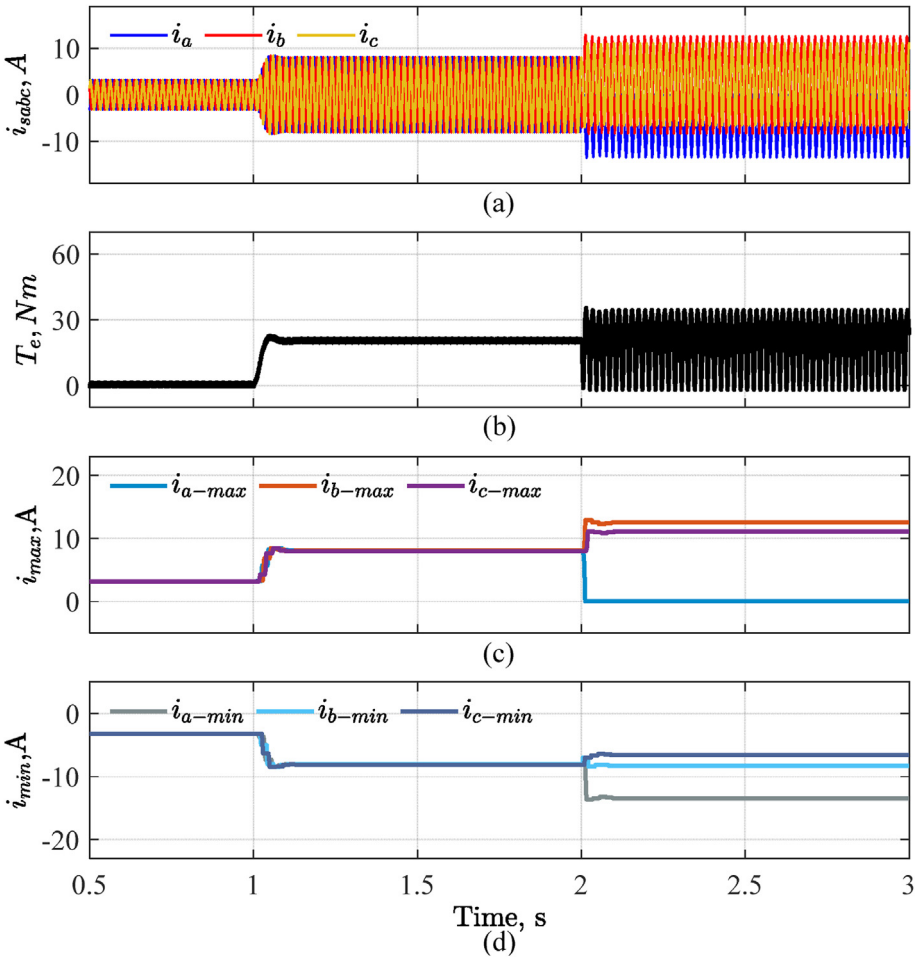

Fig. 3. Output signals due to open switch T_1 during full load. (a) Stator currents. (b) IM Torque. (c) $i_{abc-max}$. (d) $i_{abc-min}$.

the minimum value of phase *a* current reaches zero, while the remaining maximum and minimum values deviate significantly from zero. This showcases robust performance against misdiagnosis or false alarms.

The summary of the single open switch fault is depicted in Fig. 6. Generally, in cases of single open switch faults, only one of the maximum and minimum values of three-phase currents would be zero. Specifically, one of the maximum values would be zero in instances of an upper switch fault, while one of the minimum values would be zero in cases of a lower switch fault.

1.5. Double open switch located in different leg and different position, upper and lower switches

In the scenario of double open switches, where one is in the lower position and the other in the upper position, the current associated with the upper switch loses its positive half cycle, resulting in its maximum value becoming zero. Conversely, the current corresponding to the lower switch loses its negative half cycles, causing its minimum value to be zero. The magnitudes of the other maximum and minimum values increase as they move away from zero. An example of this scenario involving open switches T_1 and T_6 is depicted in Fig. 7. As illustrated in the figure, the values of i_{a-max} and i_{b-min} reach zero after the fault occurs in t = 2 s.

Figure 8 provides an overview of double open switches located in various upper and lower positions. The maximum value of the current associated with the upper open switch and the minimum value of the current related to the lower open switch are both zero. Therefore, only two values among the maximum and minimum values reach zero.

1.6. Double open switches located in different leg and in the same position, two upper or two lower switches

When two switches, situated across different legs and positioned upper, are opened, the switch

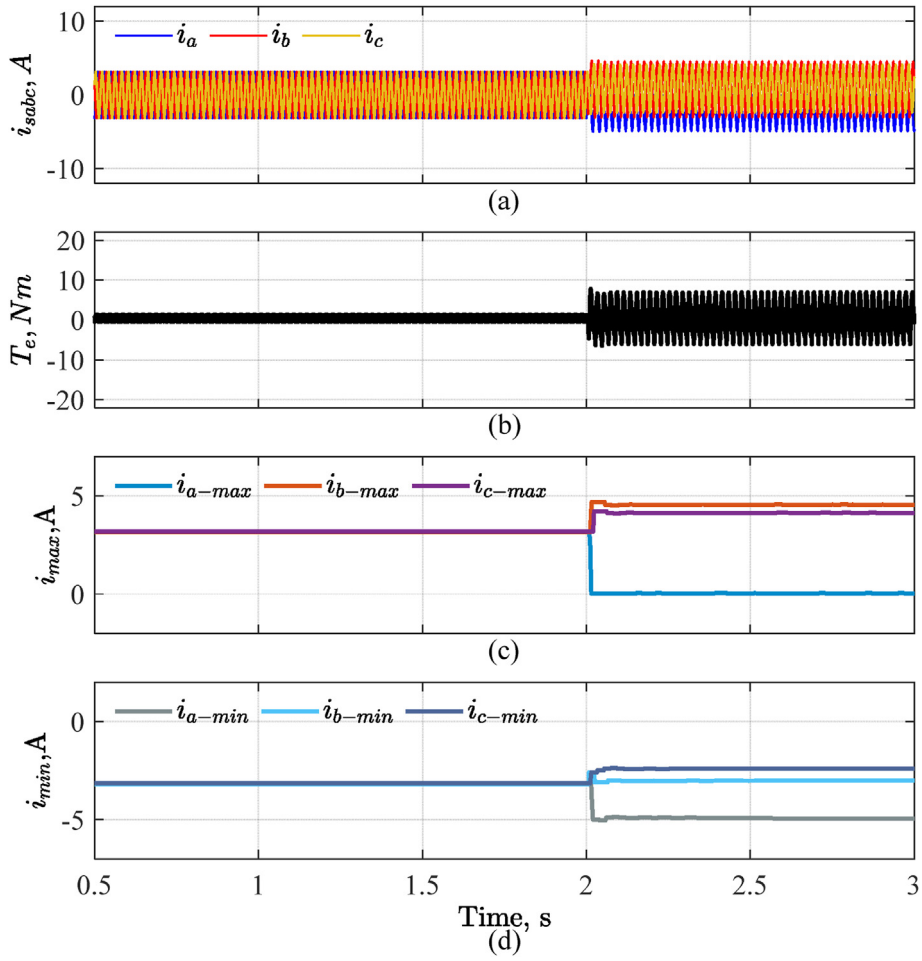

Fig. 4. Output signals due to open switch T_1 during no load. (a) Stator currents. (b) IM Torque. (c) $i_{abc-max}$. (d) $i_{abc-min}$.

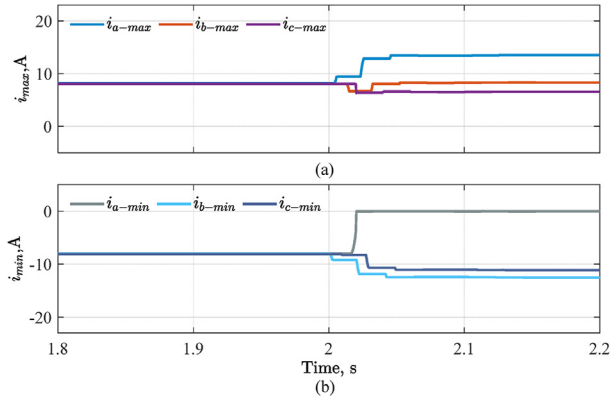

Fig. 5. Output results due to open switch T_4 during full load a) $i_{abc-max}$. b) $i_{abc-min}$.

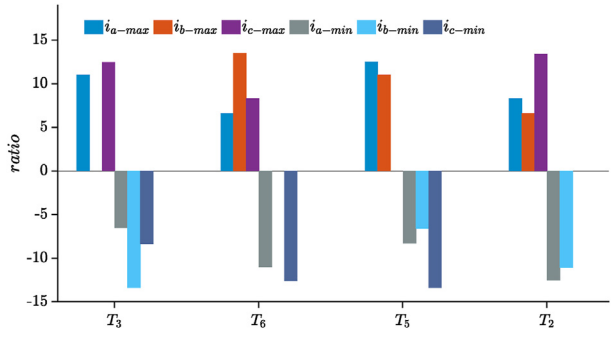

Fig. 6. Summary of $i_{abc-max}$ and $i_{abc-min}$ Values during single open switch fault cases.

located at the lower end of the third leg fails to conduct current, even though it is functioning properly. This occurs because this switch serves as the return path for the current flowing through the upper switches, which are faulted and therefore do not conduct current. Similarly, when two switches in the lower positions are open, the upper switch in the third phase fails to conduct current, resulting in the elimination of its associated half cycle. Figure 9 illustrates the maximum and minimum points of the current signals resulting from the open switches T_1 and T_3. At t = 2 s, when the fault occurs, the maximum values of current signals i_a and i_b drop to zero due to the absence of positive half cycles in

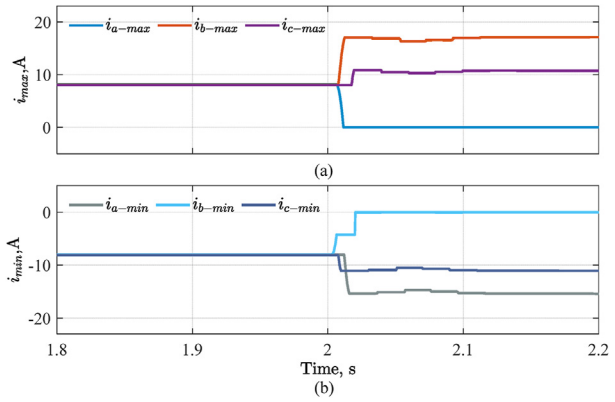

Fig. 7. Output signals due to open switches T_1 and T_6 during full load a) $i_{abc-max}$. b) $i_{abc-min}$.

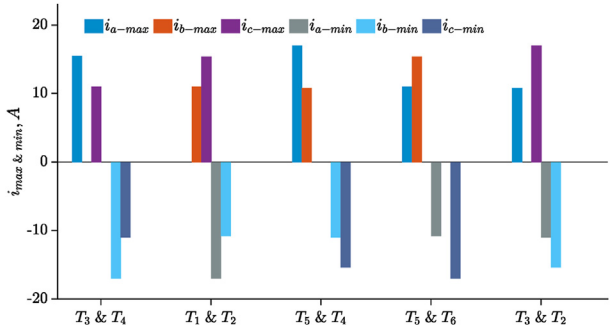

Fig. 8. Overview of $i_{abc-max}$ and $i_{abc-min}$ Values in fault cases involving double open switches in different legs, one upper and one lower.

these signals. Similarly, the minimum value of ic reaches zero as the current i_c has lost its negative cycle, as discussed earlier.

Figure 10 depicts a summary of $i_{abc-max}$ and $i_{abc-min}$ values when two switches are open at the same level, whether upper or lower. It can be seen that three out of six maximum and minimum values are zero, while the remaining variables have nonzero values.

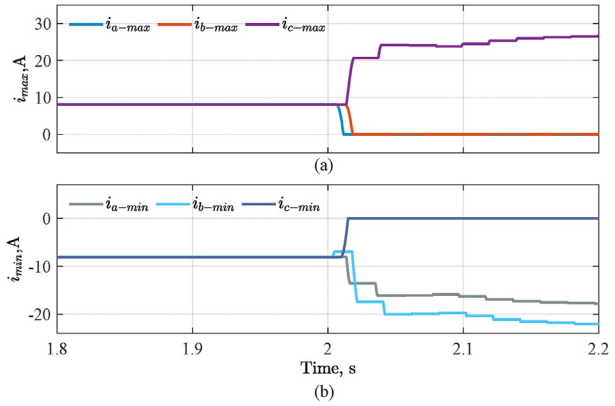

Fig. 9. Output signals due to open switches T_1 and T_3 during full load a) $i_{abc-max}$. b) $i_{abc-min}$.

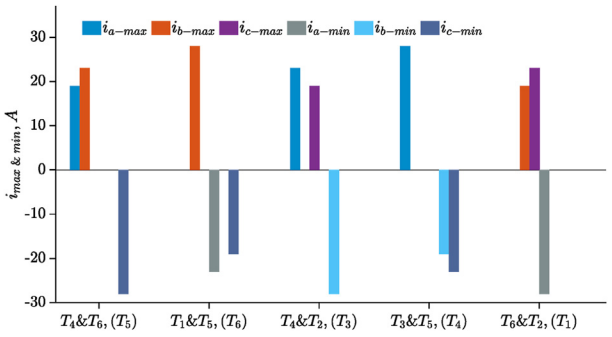

Fig. 10. Overview of $i_{abc-max}$ and $i_{abc-min}$ values in fault cases involving double open switches in different legs, either both upper or both lower.

1.7. Double open switch located in the same leg, open leg fault

When an open-leg fault occurs, the current associated with the affected leg would become zero, resulting in both the maximum and minimum values of this current signal being zero. The values of $i_{abc-max}$ and $i_{abc-min}$ when leg_1 is open are depicted in Fig. 11. The values i_{a-max} and i_{a-min} reach zero after the fault occurs at t = 2 s.

Table 2 provides an overview of diagnostic rules for open switch fault cases based on the presence or absence of zero values of $i_{abc-max}$ and $i_{abc-min}$. In the event of a single open switch fault, one of the six cases is fulfilled (i.e. one of its related max/min currents reached zero and other extracted currents

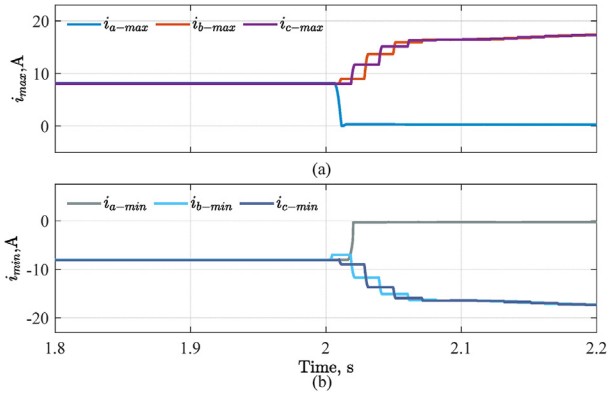

Fig. 11. Output signals due to open leg_1 (T_1 and T_4) during full load (a) $i_{abc-max}$. (b) $i_{abc-min}$.

Table 2. Diagnostic rules for open switch fault cases.

Case	i_{a-max}	i_{b-max}	i_{c-max}	i_{a-min}	i_{b-min}	i_{c-min}
T_1	0	–	–	–	–	–
T_4	–	–	–	0	–	–
T_3	–	0	–	–	–	–
T_6	–	–	–	–	0	–
T_5	–	–	0	–	–	–
T_2	–	–	–	–	–	0

will be nonzero). However, if more than one switch fault occurs, multiple cases are satisfied (i.e. more than one of max/min currents reached zero). For instance, when the values of i_{a-max} and i_{b-min} become zero, it indicates that switches T_1 and T_6 have become permanently open.

2. Experimental results

2.1. Experimental setup description

To further confirm the effectiveness of the proposed algorithm, experimentation is conducted using a 3 kW three-phase IM supplied by a two-level VSI as shown in Fig. 12. The motor is regulated to operate under constant V/f control, set to 70% of the rated voltage and frequency. This control setup is implemented using a Texas Instruments TMS320C6713 DSP, coupled with Actel FPGA A3P400-based boards and host port interface (HPI) daughter cards. Motor current is measured using LEM LA 100-P current transducers and captured through a data acquisition board integrated with LabView. The current data is recorded over 10 s,

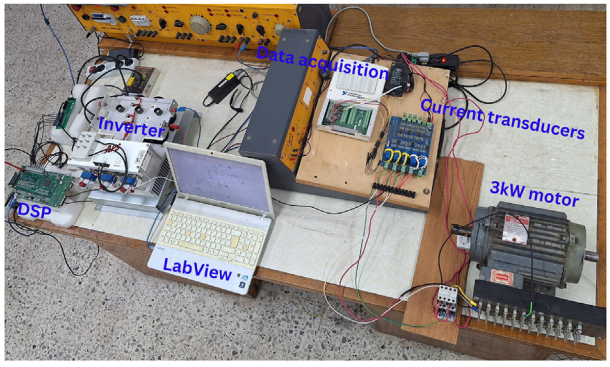

Fig. 12. Experimental setup.

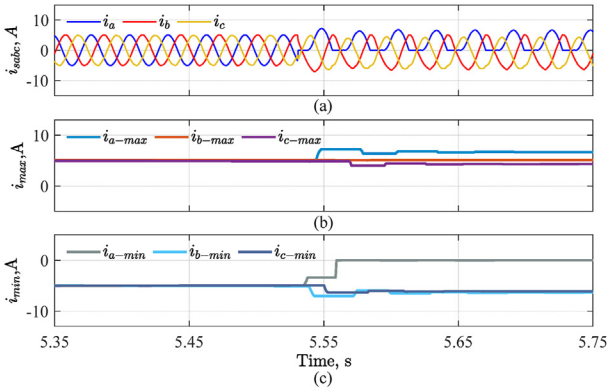

Fig. 13. Experimental signals due to open switch T_4 (a) Stator currents. (b) $i_{abc-max}$. (c) $i_{abc-min}$.

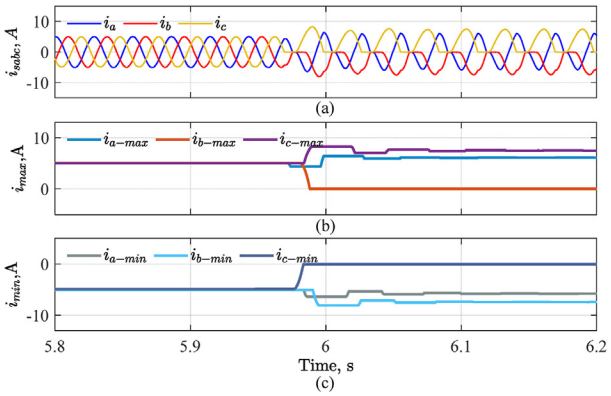

Fig. 14. Experimental signals due to open switches T_3 and T_2 (a) Stator currents. (b) $i_{abc-max}$. (c) $i_{abc-min}$.

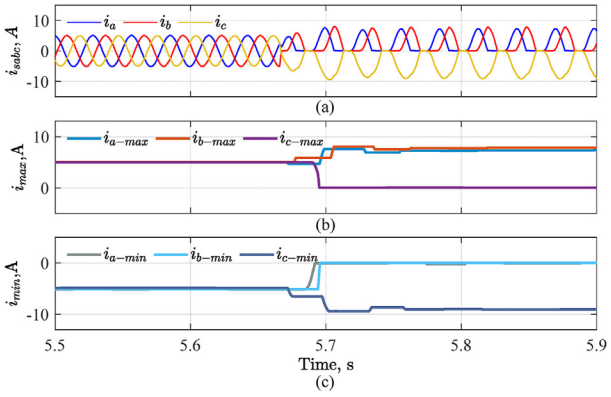

Fig. 15. Experimental results due to open switches T_4 and T_6 (a) Stator currents. (b) $i_{abc-max}$. (c) $i_{abc-min}$.

after which the proposed algorithm is applied using a MATLAB subroutine.

2.2. Experimental results discussion

During the experimental tests, the motor is running under no load and the open switch faults

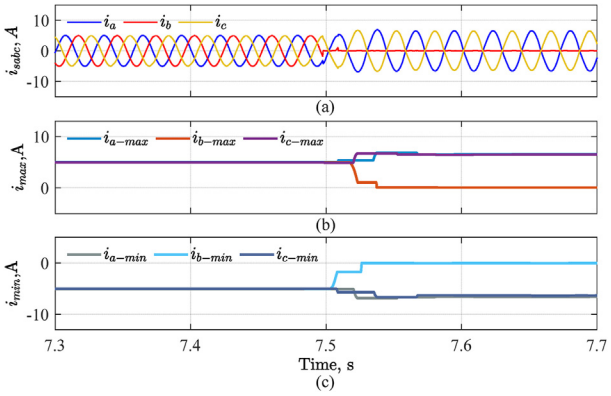

Fig. 16. Experimental results due to open leg$_2$ (T_3 and T_6) a) Stator currents. b) $i_{abc-max}$. c) $i_{abc-min}$.

Table 3. Comparison with previous approaches.

Case	Yu et al. (2014)	Zhou et al. (2022)	Suti and Di Rito (2024)	Proposed method
Fault diagnosis cases	18	9	6	21
Consider changes in the load.	Yes	Yes	No	Yes
Computational complexity	Medium	High	High	Low
Dependence of threshold	Yes	Yes	Yes	No
Robustness against false alarm	High	Low	High	High
Diagnosis time	2–3 T	1.3 T	$< 0.5\,T$	$0.5 - 1\,T$

are intentionally carried out. A selected four cases are present as follows:

Figure 13 illustrates the three-phase current signals along with their respective maximum and minimum values when the lower switch T_4 is open. As previously mentioned, i_a signal loses its negative half-cycle, causing the value of i_{a-min} to drop to zero. It is apparent that the signal waveforms bear similarities when juxtaposed with their simulated counterparts depicted in Fig. 5.

The fault scenario, involving the double open switches T_3 (an upper switch) and T_2 (a lower switch), is depicted in Fig. 14. As depicted in Fig. 14a, the current signal i_b loses its positive half cycle due to the open switch T_3, while the signal i_c loses its negative half cycle due to the open switch T_2. Consequently, the values of i_{b-max} and i_{c-min} both reach zero, as illustrated in Fig. 14b and c, respectively.

When the lower switches T_4 and T_6 are open, the negative half cycles of current signals i_a and i_b are eliminated, along with the positive half cycle of current is as discussed in Subsection IV-C. Consequently, the values of i_{a-min}, i_{b-min} and i_{c-max} all change to zero as shown in Fig. 15.

In the case of open switches T_3 and T_6, which are in the same leg, their respective current signal i_b is completely lost and becomes zero. Consequently, both the values of i_{b-max} and i_{b-min} become zero as shown in Fig. 16.

2.3. Comparison with previous approaches

Table 3 provides a comparison with open switch fault diagnosis. The assessment criteria including number of fault cases can be detected, load variation considerations, complex computational requirements, threshold dependence. Robustness against false alarm and detection time. The proposed methodology clearly demonstrates superiority over alternative approaches in most evaluation criteria. While the method presented in Suti and Di Rito (2024) exhibits faster fault detection time, it is limited to identifying only six single open switch cases.

3. Conclusion

This paper presents a novel approach for detecting open-switch faults in a three-phase PWM-VSI system fed an IM, based on signal current maximum and minimum points. The proposed method utilizes motor phase currents already being measured for speed control purposes, eliminating the need for additional sensors, which enhances cost-effectiveness. Several test scenarios were conducted, including single open-switch faults, double open-switch faults, and open-phase faults. Simulation and experimental results demonstrate that the proposed method yields clear indicators that efficiently and promptly identify the open switch(es) without requiring complex calculations or additional hardware. Furthermore, the proposed method can seamlessly integrate with existing electric drive systems via its programmed control/troubleshooting electronic boards in future motor drive designs.

Author's contribution

The corresponding author is responsible for experimental investigations and writing the manuscript. The second author is responsible for discussing the results, and revision. The third author is responsible for software simulation and helping with the writing of the manuscript.

Conflicts of interest

There are no conflicts of interest.

References

An, Q., Sun, L., Sun, L., 2013. Hardware-circuit-based diagnosis method for open-switch faults in inverters. Electron letters 49, 1089–1091.

Chen, K., Ji, S.M., Zhang, L., 2016. Two-level three-phase voltage source inverter fed low-power AC induction motor based on unipolar pulse-width modulation method. IET Power Electron. 9, 435–440.

Cheng, Y., Sun, Y., Li, X., Dan, H., Lin, J., Su, M., 2020. Active common-mode voltage-based open-switch fault diagnosis of inverters in IM-drive systems. IEEE Trans. Ind. Electron. 68, 103–115.

Eltamaly, A.M., Alolah, A.I., Badr, B.M., 2010. Fuzzy controller for three phases induction motor drives. In: 2010 International Conference on Autonomous and Intelligent Systems, AIS 2010. IEEE, Povoa de Varzim, Portugal, pp. 1–6.

Eltamaly, A.M.A., 2020. Improved control strategy for three-phase ac choppers under induction motor load. Mansoura Eng. J. 32, 86–92.

Georgakopoulos, I.P., Mitronikas, E.D., Safacas, A.N., 2010. Detection of induction motor faults in inverter drives using inverter input current analysis. IEEE Trans. Ind. Electron. 58, 4365–4373.

Guan, Y., Sun, D., He, Y., 2007. Mean current vector based online real-time fault diagnosis for voltage source inverter fed induction motor drives. In: 2007 IEEE International Electric Machines & Drives Conference. IEEE, pp. 1114–1118.

Huang, Z., Wang, Z., Yao, X., Zhang, H., 2018. Multi-switches fault diagnosis based on small low-frequency data for voltage-source inverters of PMSM drives. IEEE Trans. Power Electron. 34, 6845–6857.

Jiang, C., Li, S., Habetler, T.G., 2017. A review of condition monitoring of induction motors based on stray flux. In: 2017 IEEE energy conversion congress and exposition (ECCE). IEEE, pp. 5424–5430.

Jlassi, I., Cardoso, A.J.M., 2019. A single method for multiple IGBT, current, and speed sensor faults diagnosis in regenerative PMSM drives. IEEE J. Emerg. Sel. Top. Power Electron. 8, 2583–2599.

Khomfoi, S., Tolbert, L.M., 2007. Fault diagnostic system for a multilevel inverter using a neural network. IEEE Trans. Power Electron. 22, 1062–1069.

Mamat, M.R., Rizon, M., Khanniche, M., 2006. Fault detection of 3-phase VSI using wavelet-fuzzy algorithm. Am. J. Appl. Sci. 3, 1642–1648.

Shabbir, M.N.S.K., Liang, X., Chakrabarti, S., 2020. An ANOVA-based fault diagnosis approach for variable frequency drive-fed induction motors. IEEE Trans. Energy Convers. 36, 500–512.

Shadlu, M.S., 2017. Fault detection and diagnosis in voltage source inverters using principle component analysis. In: 2017 IEEE 4th International Conference on Knowledge-Based Engineering and Innovation (KBEI). IEEE, pp. 509–515.

Sun, X., Song, C., Zhang, Y., Sha, X., Diao, N., 2023. An open-circuit fault diagnosis algorithm based on signal normalization preprocessing for motor drive inverter. IEEE Trans. Instrum. Meas.

Suti, A., Di Rito, G., 2024. Diagnosis of power switch faults in three-phase permanent magnet synchronous motors via current-signature technique. Actuators 13 (1), 25. MDPI.

Trabelsi, M., Boussak, M., Benbouzid, M., 2017. Multiple criteria for high performance real-time diagnostic of single and multiple open-switch faults in ac-motor drives: Application to IGBT-based voltage source inverter. Elec. Power Syst. Res. 144, 136–149.

Tran, C.D., Palacky, P., Kuchar, M., Brandstetter, P., Dinh, B.H., 2021. Current and speed sensor fault diagnosis method applied to induction motor drive. IEEE Access 9, 38660–38672.

Wang, Y., Li, Z., Xu, M., Ma, H., 2016. A comparative study of two diagnostic methods based on the switching voltage pattern for IGBT open-circuit faults in voltage-source inverters. J. Power Electron. 16, 1087–1096.

Wang, B., Feng, X., Sun, T., Wang, Z., Cheng, M., 2023. Relative β-axis residual voltage signal based fault detection for inverter switch open-circuit failure. IEEE Trans. Power Electron. 38, 11315–11326.

Wu, F., Zhao, J., 2015. A real-time multiple open-circuit fault diagnosis method in voltage-source-inverter fed vector controlled drives. IEEE Trans. Power Electron. 31, 1425–1437.

Xu, X., Yu, F., 2022. A switch open-circuit fault diagnosis method for three-phase inverters based on voltage patterns. In: 2022 2nd International Conference on Electrical Engineering and Control Science (IC2ECS). IEEE, pp. 901–908.

Yan, H., Peng, Y., Shang, W., Kong, D., 2023. Open-circuit fault diagnosis in voltage source inverter for motor drive by using deep neural network. Eng. Appl. Artif. Intell. 120, 105866.

Yang, S., Bryant, A., Mawby, P., Xiang, D., Ran, L., Tavner, P., 2011. An industry-based survey of reliability in power electronic converters. IEEE Trans. Ind. Appl. 47, 1441–1451.

Yang, H., Peng, Z., Xu, Q., Huang, T., Zhu, X., 2023. Inverter fault diagnosis based on Fourier transform and evolutionary neural network. Front. Energy Res. 10, 1090209.

Yu, Y., Hu, J., Wang, Z., Xu, D., 2014. IGBT open circuit fault diagnosis in VSI fed induction motor drives based on modified average current method. In: 2014 9th IEEE Conference on Industrial Electronics and Applications. IEEE, pp. 1334–1338.

Zhou, X., Sun, J., Cui, P., Lu, Y., Lu, M., Yu, Y., 2020. A fast and robust open-switch fault diagnosis method for variable-speed PMSM system. IEEE Trans. Power Electron. 36, 2598–2610.

Zhou, Y., Zhao, J., Song, Y., Sun, J., Fu, H., Chu, M., 2022. A seasonal–trend-decomposition-based voltage-source-inverter open-circuit fault diagnosis method. IEEE Trans. Power Electron. 37, 15517–15527.